# Polar Embedded Catmull-Clark Subdivision Surface

Anonymous submission

**Abstract**

In this paper, a new subdivision scheme with Polar embedded Catmull-Clark mesh structure is presented. In this new subdivision scheme, the control mesh divides into two parts, quadrilateral part (CCS) and triangular part (Polar), and one can generate limit surfaces which are exactly the same as those of CCS on quad part and $G^2$ on triangular part. The common ripple effect surrounding high-valence extraordinary points in CCS surface is improved by replacing high-valence CCS extraordinary faces with triangular Polar faces. The new scheme is valence independent and stationary. By using the same subdivision masks on both CCS part and Polar part, the artifact of earlier researches (mismatch of subdivision masks, exponential subfaces at $n^{th}$ subdivision level) is resolved. Test results show that, with the new scheme, one can generate very high quality, curvature continuous subdivision surfaces on the Polar part. Together with current available CCS $G^2$ schemes, one can generate high quality subdivision surfaces appropriate for most engineering applications.

*Keywords:*

## 1. Introduction

Subdivision surfaces have been widely used in CAD, gaming and computer graphics. Catmull-Clark subdivision (CCS) [1], based on tensor product bi-cubic B-Splines, is one of the most important subdivision schemes. The surfaces generated by the scheme are $C^2$ continuous everywhere except at extraordinary points, where they are $C^1$ continuous.

The works of Doo and Sabin [2] , and Stam [3] illustrate the behavior of a CCS surface at extraordinary points. Much research has been performed to improve the curvature surrounding extraordinary points. Prautzsch [4] modifies the scheme to generate zero curvature at extraordinary points. Levin [5] gives a scheme to generate a $C^2$ continuous surface at extraordinary points by blending the surface with a low degree polynomial. Karčiauskas, K. and Peters [6] present a guided scheme, which fills a series of subsequently $\lambda$-scaled surface rings to an N-sided hole. Loop and Schaefer [7] present a second order smooth filling of an N-valence Catmull-Clark spline ring with N bi-septic patches.

A shortcoming inherent in CCS surfaces is the ripple problem, that is, ripples tend to appear around extraordinary points with high valence. In the past, research focused on improving the curvature at extraordinary points. However, with quad mesh structure of CCS surfaces, the ripples could not be avoided in high

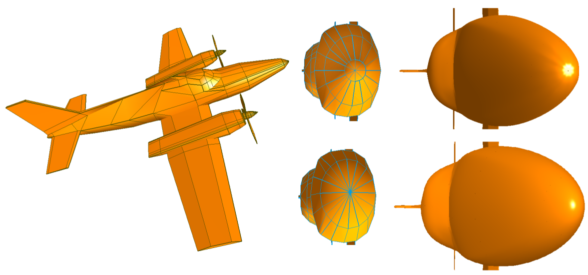

Figure 1: Left: original CCS mesh for an airplane. Right: the top shows the limit surface and the original CCS mesh for the head of plane, with zero curvature on the tip, the bottom shows the limit surface and the new mesh with a high valence Polar extraordinary point on the plane head, with non-zero curvature and $G^2$ on the tip of the plane head.

valence cases. The technique of fairing [8] is used to address the smoothness issue on the limit surface, but the computation is quite expensive and it changed the limit surface to the extent that it does not generate the desired shape.

To handle this artifact, Polar surface has been studied by a number of researchers. Polar surface has a quad/triangular mixed mesh structure. [9] shows a guided subdivision scheme that uses a Bezier surface as a guide for each subdivision step, and a $C^2$ accelerated bi-cubic guided subdivision that uses $2^m$ subfaces in the $m^{th}$ level for surface patches surrounding extraordinary points. In the second case, they show that although this scheme is not practical for CCS surfaces, it can be applied in a Polar configuration. A bi-cubic Polar subdivision scheme is presented in [10] that sets up the control mesh refinement rules for Polar configuration so that the limit surface is $C^1$ continuous and curvature bounded. As a further step, Myles and Peters [11] presented a bi-cubic $C^2$ Polar subdivision scheme that gets a $C^2$ Polar surface by modifying the weights of Polar subdivision scheme for different valences.

Although a Polar surface handles high valence cases well, there are issues preventing its application in subdivision surfaces. Mismatch of subdivision masks between Polar and CCS makes it difficult to connect Polar to CCS meshes . Although in [12], the effort is made to connect Polar to CCS meshes. The scheme suffers the problem of inconsistent limit surfaces with refined control mesh at different subdivision levels, and it generates $2^m$ CCS subfaces in the $m^{th}$ level.

A free-form quad/triangular scheme was presented in [13], [14] and [15]. However, the scheme was not designed to handle high-valence ripples as Polar surface.

In this paper, we redefined a quad/tri mesh structure, named the Polar Catmull-Clark mesh (PCC mesh), which embeds Polar configuration into the Catmull-Clark mesh structure to solve the high valence issue. A new subdivision scheme is developed on PCC mesh.

In contrast to the work in [12], our new scheme has the equivalent subdivision masks on both Polar and CCS parts, such that there are no mismatches of subdivision rules on the boundaries between Polar and CCS parts and avoid the artifact of inconsistent limit surface at different subdivision levels. The scheme will generate $2m$ CCS subfaces at $m^{th}$ subdivision level which makes parameterization possible. We also show that the generated limit surface on triangular part is $G^2$ at extraordinary points and the artifact of high valence ripples is resolved effectively. Fig 1 shows a CCS control mesh of an airplane, at the plane head, although one has tried to avoid ripples by adding a flat area on the tip, ripples still appear at the surrounding area. With the mesh modified to embed a Polar configuration at plane head, by our new $G^2$ scheme on Polar part, ripples are eliminated and generates non-zero curvature on the tip of the plane head.

The rest of the paper is organized as follows. Section 2 discusses the earlier works, Section 3 covers preprocessing of PCC mesh, Section 4 introduces Guided U-Subdivision and its construction, Section 5 applies the scheme to Polar parts of the new control mesh, Section 6 evaluates behavior of the limit surfaces around extraordinary points of the Polar parts, Section 7 concludes.

## 2. Earlier works of Polar Catmull-Clark Mesh

In this section, we introduce the earlier works on Polar Catmull-Clark (PCC) mesh.

CCS works on arbitrary topology. The subdivision requires all quad faces with no extraordinary points neighbor to each other, which is obtained by twice subdivision on original mesh [1]. Polar surfaces have the following properties on mesh structure: faces adjacent to the extraordinary points are triangular, all other faces are regular [9] [10] [16]. Fig 2 left and middle show typical meshes of Polar and Catmull-Clark respectively.

Since Polar mesh has a special mesh structure, all faces are arranged radially, so it will not work on arbitrary topology. Efforts are made to combine Polar with Catmull-Clark mesh [12]. Fig 1 right shows a typical Polar embedded Catmull-Clark mesh, which allows extraordinary points also in quad mesh part. In this paper, we develop our new subdivision scheme on this mesh structure named Polar Catmull-Clark (PCC) mesh.

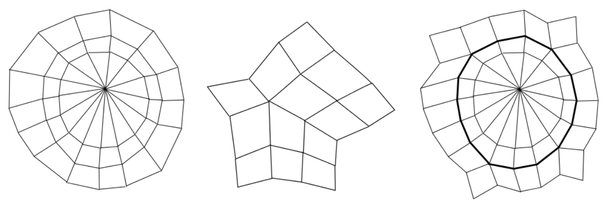

Figure 2: From left to right, Polar mesh, CCS mesh, and PCC mesh.

A PCC mesh is flexible to design, and works on arbitrary topology. Given an arbitrary control mesh, one just subdivides it twice to generate a control mesh suitable for further CCS [1] [17], then analyze the mesh and find out where one wants to put Polar structure, typically for high valence extraordinary faces. By taking out these extraordinary faces and replacing them with triangular/quad meshes (inside the bold edges on the right of Fig 2), one obtain a PCC mesh.

In an earlier effort to handle PCC mesh by Myles' work [12], to connect Polar and CCS, it has 4 steps to process the Polar part. 1) separate subdivision into two parts, 2) performing k times subdivision radially and then k times circularly, 3) performing k times subdivision on remaining CCS mesh, 4) merge boundaries set by 2) and 3). This algorithm suffers the problem that the limit surface of the merged control mesh will be different with different subdivision levels. By analyzing its algorithm, one can find this artifact is caused by mismatch between subdivision masks for Polar parts and CCS parts. This artifact needs to be resolved, since in CAGD and other high precision graphics applications, limit surface is generally required to be unchanged with refined control meshes. Also at $k^{th}$ subdivision level, one has to handle undesired $2^k$ CCS subfaces.

We have the following research question naturally arise: *Can we develop a subdivision scheme to process the Polar part of PCC mesh, such that subdivision mask is the same as the CCS part to form a natural $C^2$ join between Polar part and CCS part, and only $O(n)$ subfaces generated at the $n^{th}$ subdivision level?*

To achieve this goal, we need to develop a new subdivision scheme for Polar part.

## 3. Preprocessing of PCC mesh

The valence of a Polar extraordinary point in a PCC mesh can be even or odd.

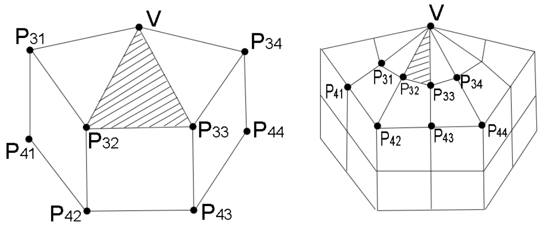


Figure 3: convert Polar odd valence to even by one subdivision

Since for odd valence, the curvature continuity is more difficult to achieve than even cases, before we work on Polar part, we need to convert odd valence to even. Performing one CCS so that the new extraordinary point will have an even valence (as shown on right side of Fig. 3). In this subdivision, each triangular face will be treated as a quad face by vertex splitting of Polar extraordinary point $V$ (see Fig 4). The new edge and face points of triangular faces are defined by CCS rules, but for a new vertex point, we use the original CCS vertex point rule on arbitrary topology [1] by $V' = \frac{N-2}{N}V + \frac{1}{N^2}\sum_{i=1}^{N} E_i + \frac{1}{N^2}\sum_{i=1}^{N} F'_i$.

Above we introduced the preprocessing of a PCC mesh structure to convert all Polar extraordinary points to even valence. The next section will focus on our new scheme to handle Polar part.

## 4. Guided U-Subdivision

In preprocessing of PCC mesh, triangular face is treated as a quad face with two control points coincides.

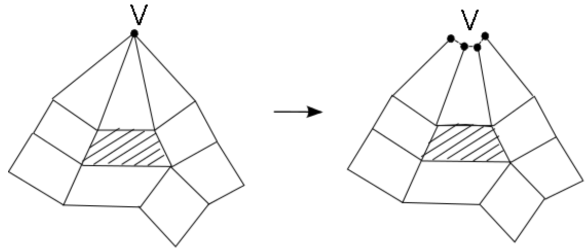


Figure 4: Control mesh conversion for triangular faces adjacent to an extraordinary point.

If we can find a CCS equivalent radially recursive subdivision scheme to work on triangular faces after vertex splitting, then it is possible to avoid mismatch between Polar and CCS. The limit surface generated will be $C^2$ between Polar and CCS parts without exponential number of subfaces at $n^{th}$ level.

In this section, we first introduce a CCS equivalent subdivision scheme, the U-Subdivision. Then we present a Guided U-Subdivision (GUS). With GUS, we will be able to generate a $G^2$ limit surface on Polar part of a PCC mesh. Our new subdivision scheme has the equivalent subdivision mask with neighboring CCS, such that one can generate a $C^2$ natural join between Polar part and CCS part.

### *4.1. U-Subdivision*

Recall that the CCS scheme divides the control vertices into three categories: *vertex points*, *edge points*, and *face points*. A popular way to index the control vertices is shown in Fig 5, where $V$ is a vertex point, $E_i$'s are edge points, $F_i$'s are face points and $I_{i,j}$'s are inner ring control vertices. New vertices within each subdivision step are generated as follows:

$$
\begin{aligned}
V' &= \alpha_N V + \beta_N \sum_{i=1}^{N} E_i/N + \gamma_N \sum_{i=1}^{N} F_i/N \\
E'_i &= \frac{3}{8}(V + E_i) + \frac{1}{16}(E_{i+1} + E_{i-1} + F_i + F_{i-1}) \\
F'_i &= \frac{1}{4}(V + E_i + E_{i+1} + F_i)
\end{aligned}
\tag{1}
$$

where $N$ is the valence of vertex $V$, with $\alpha_N = 1 - \frac{7}{4N}$, $\beta_N = \frac{3}{2N}$, *and* $\gamma_N = \frac{1}{4N}$.

A regular bi-cubic B-spline patch with parameters $u$ and $v$ can be expressed as

$$S(u, v) = [1\ u\ u^2\ u^3]\ M\mathbf{P}M^T\ [1\ v\ v^2\ v^3]^T \tag{2}$$

where $\mathbf{P}$ is a $4\times4$ matrix of control points $P_{ij}$, $1 \le i, j \le 4$, $M$ is the coefficient matrix and $M^T$ is its transpose.

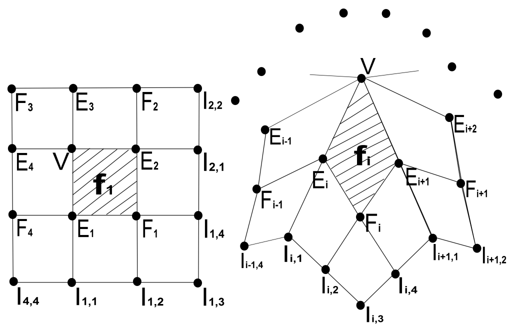


Figure 5: Control meshes of Catmull- Clark subdivision. Left side: a regular face; right side: an extraordinary face

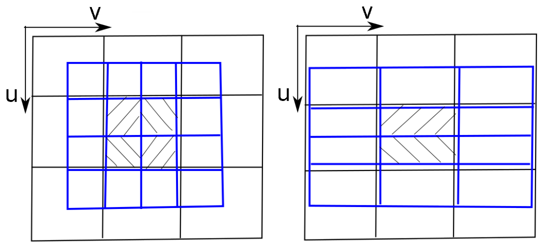


Figure 6: Left is a CCS, right is a U-Subdivision

The subdivision process of control points are obtained by subdivision rules shown in (1).

We notice that CCS on a regular face can be expressed as first to subdivide in $u$ direction then in $v$ direction. If the subdivision in $v$ direction is dropped, we obtain a CCS equivalent subdivision surface involving parameter $u$ only, named unilateral subdivision (U-Subdivision), with subdivision rules as follows:

$$\begin{aligned} V' &= \frac{3}{4}V + \frac{1}{8}E_1 + \frac{1}{8}E_3 \\ E_i' &= \frac{1}{2}V + \frac{1}{2}E_i \end{aligned} \tag{3}$$

A U-Subdivision splits a regular CCS patch into two regular CCS sub-patches.

**PROPERTY 1** : The limit surfaces of the two CCS sub-patches generated by a U-Subdivision are the same as the limit surface of that regular patch.

*Proof* : The two sub-patches generated by a U-Subdivision can be expressed as follows:

$$S_b(\bar{u}, \bar{v}) = [1\ \bar{u}\ \bar{u}^2\ \bar{u}^3]\ MA_b\mathbf{P}M^T\ [1\ \bar{v}\ \bar{v}^2\ \bar{v}^3]^T \tag{4}$$

where $b = 1, 2$, $(\bar{u}, \bar{v})$ takes value from $[0, 1] \times [0, 1]$, $A_1$ and $A_2$ are U-Subdivision matrices for the 1st and the 2nd sub-patches, respectively. For the 1st sub-patch, because

$$[1\ \bar{u}\ \bar{u}^2\ \bar{u}^3]\ MA_1 = [1\ \frac{1}{2}\bar{u}\ \frac{1}{4}\bar{u}^2\ \frac{1}{8}\bar{u}^3]\ M$$

we can express the sub-patch as

$$S_1(\bar{u}, \bar{v}) = [1\ \frac{1}{2}\bar{u}\ (\frac{1}{2}\bar{u})^2\ (\frac{1}{2}\bar{u})^3]\ M\mathbf{P}M^T\ [1\ \bar{v}\ \bar{v}^2\ \bar{v}^3]^T$$

which is exactly the first half of the original $(u, v)$ regular patch. Similarly, we can see that the 2nd sub-patch represents the 2nd half of the original patch. QED

Consequently, we can prove that after n times U-Subdivision, the limit surfaces of $2^n$ U-subdivided sub-patches are the same as the original CCS limit surface.

### *4.2. Guided U-Subdivision*

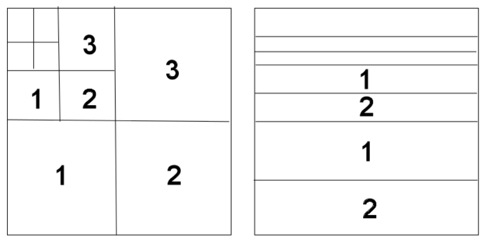


Figure 7: Ω-Partitions, left for Catmull-Clark, right for GUS

In this section, we show how to perform a guided U-Subdivision (GUS) and how to obtain a GUS surface.

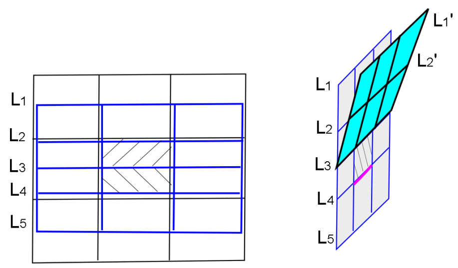


Figure 8: Left side shows 5 layers in a U-Subdivision, right shows $L_1$ and $L_2$ will not change boundary (red) continuity.

For a regular patch, if we do a U-Subdivision, we get 2 sub-patches with 20 control points. These points are distributed in 5 layers, with four points each. We denote them $L_1$, $L_2$, $L_3$, $L_4$ and $L_5$, respectively (as shown in

Fig 5).

**PROPERTY 2**: Only $L_3$ ,$L_4$, and $L_5$ obtained after a U-Subdivision on a regular patch are needed to ensure $C^2$ continuity of the limit surface on the common boundary with an adjacent patch underneath it.

*Proof* : This property is trivial in CCS and can be derived from analysis of equation (2). QED

This gives us an opportunity to set up a recursive subdivision scheme that takes $L_3$, $L_4$, and $L_5$ from a U-Subdivision on previous control mesh, but leaves $L_1$ and $L_2$ at the user's choice, so that the shape of the limit surface can be guided by the selected $L_1$ and $L_2$.

Given an arbitrary regular patch with a $4 \times 4$ control point mesh $\mathbf{P}$, we define the limit surface $S(u, v)$ of a GUS surface as the union of recursively generated U-Subdivision surfaces $S_{n,b}(\bar{u}, \bar{v})$ (limit surface of $n^{th}$ GUS and $b^{th}$ sub-patch), with an $\Omega$-partition (see Fig. 7) defined as follows:

$$\Omega_{n,1} = [\frac{1}{2^n}, \frac{3}{2^{n+1}}] \times [0, 1], \quad \Omega_{n,2} = [\frac{3}{2^{n+1}}, \frac{1}{2^{n-1}}] \times [0, 1]$$

Hence, each GUS will generate 2 regular sub-patches which require 5 layers of 20 control points. The GUS process is shown below.

For this given regular patch, we need to define a $5 \times 4$ basis control mesh $\mathbf{P}^0$ for the GUS first. The first three layers of $\mathbf{P}^0$ are obtained by performing a U-Subdivision on the last three layers of $\mathbf{P}$ and the last two layers of $\mathbf{P}^0$ are zero, i.e.,

$$\mathbf{P}^0 = \begin{bmatrix} A_3 P'_{3,4}\mathbf{P} \\ 0 \end{bmatrix}, \qquad with\ A_3 = \begin{bmatrix} \frac{1}{4} & \frac{1}{4} & 0 \\ \frac{1}{8} & \frac{3}{4} & \frac{1}{8} \\ 0 & \frac{1}{4} & \frac{1}{4} \end{bmatrix} \quad (5)$$

and $P'_{3,4}$ is a $3{\times}4$ picking matrix with $I_3$ ( identity matrix of size 3) on the right side of the matrix.

For each $n \geq 1$, let $\mathbf{P}^n$ be the $5{\times}4$ control point matrix of the $n^{th}$ GUS with layers $L_i^n$, $1 \leq i \leq 5$. The last three layers $L_3^n$, $L_4^n$ and $L_5^n$ of $\mathbf{P}^n$ are obtained by performing a $U$-subdivision on the first three layers $L_1^{n-1}$, $L_2^{n-1}$ and $L_3^{n-1}$ of $\mathbf{P}^{n-1}$, i.e.,

$$P'_{3,5}\mathbf{P}^n = A_3 P_{3,5}\mathbf{P}^{n-1}, \quad n \geq 1 \qquad (6)$$

where $P_{3,5}$ and $P'_{3,5}$ are $3 \times 5$ picking matrices with $I_3$ on the left and right side of the matrix, respectively. The first two layers $L_1^n$ and $L_2^n$ of $\mathbf{P}^n$ are at the choice of the user (the selection criteria of these two layers will be discussed in Section 4 for a Polar configuration). Once these two layers have been selected, the control point computation process for the $n^{th}$ GUS is complete.

**THEOREM 1:** Control points in $L_1^n$ and $L_2^n$ of the control point matrix $\mathbf{P}^n$ of an $n^{th}$ GUS surface can be changed without affecting $C^2$ continuity of the limit surface inside the parameter space and on the boundary $(u = 1)$ with its adjacent regular patch.

*Proof* : For $\mathbf{P}^n$ of an $n^{th}$ GUS surface, its $L_3^n$, $L_4^n$ and $L_5^n$ are obtained by doing one U-Subdivision on the $1^{st}$ three layers of $\mathbf{P}^{n-1}$, by Property 2, it is $C^2$ continuous at the boundary with previous GUS patch. Within an $n^{th}$ GUS surface, $C^2$ continuity is trivial. QED

With all control points in $\mathbf{P}^n$ defined, we can now define the GUS surface. For any $(u, v) \in [0, 1] \times [0, 1]$, where $(u, v) \neq (0, v)$, there is an $\Omega_{n,b}$ containing $(u, v)$. We can find the value of $S(u, v)$ by mapping $\Omega_{n,b}$ to the unit square $[0, 1] \times [0, 1]$ and finding the corresponding point of $(u, v)$ in the unit square: $(\overline{u}, \overline{v})$, then compute $S_{n,b}$ (the limit surface of $n^{th}$ GUS and $b^{th}$ sub-patch) at $(\overline{u}, \overline{v})$. The value of $S(0, v)$ is the limit of the GUS.

In the above process, n and b can be computed by:

$$n(u, v) = \lceil \log_{\frac{1}{2}} u \rceil$$

$$b(u, v) = \begin{cases} 1, & \text{if } 2^n u \leq 1.5 \\ 2, & \text{else} \end{cases}$$

The mapping from $\Omega_{n,b}$ to the unit square is defined as $(\overline{u}, \overline{v}) = (\phi(u), v)$ , with

$$\phi(u) = \begin{cases} 2^{n+1}u - 2, & \text{if } 1.5 \geq 2^n u > 1 \\ 2^{n+1}u - 3, & \text{if } 2^n u > 1.5 \end{cases}$$

The limit surface $S(u, v)$ can be defined as follows:

$$S(u, v) = W^T(\bar{u}) M \mathbf{P}^{n,b} M^T W(\bar{v}) \qquad (7)$$

where $\mathbf{P}^{n,b}$, a $4 \times 4$ matrix, contains the 16 control points of $S_{n,b}$, with $\mathbf{P}^{n,1} = S_1\mathbf{P}^n$ and $\mathbf{P}^{n,2} = S_2\mathbf{P}^n$, $S_1$ and $S_2$ are picking matrices of size $4 \times 5$ with $I_4$ (identity matrix of size 4) on the left and right side of the matrix respectively. $W(x)$ is the 4-component power basis vector with $W^T(x) = [1, x, x^2, x^3]$, M is the B-spline curve coefficient matrix. We can express $W^T(\overline{u})$ and $W^T(\overline{v})$ as follows

$$W^T(\overline{u}) = W^T(u) K^{n+1} D_b, \qquad W^T(\overline{v}) = W^T(v)$$

where K is a diagonal matrix, with $K = Diag(1, 2, 4, 8)$. $D_b$ is an upper triangular matrix depending on b only, it maps $(\overline{u}, \overline{v})$ to $(u, v)$. So we can rewrite the subdivision surface as

$$S(u, v) = W^T(u) K^{n+1} D_b M S_b \mathbf{P}^n M^T W(v) \qquad (8)$$

Thus we can decompose the limit surface into a sequence of recursively generated U-Subdivision surfaces,

$S(u, v) = S_{1,2} \cup S_{1,1} \cup S_{2,2} \cup S_{2,1} \cup S_{3,2} \cup ...$

In the above, we have shown the construction of a GUS surface and proven its $C^2$ continuity both inside the limit surface and on the boundary of $u = 1$. In the following section, we show how this subdivision scheme can be applied to the Polar configuration.

## 5. Applying GUS to Polar Parts

After preprocessing of PCC mesh (section 3), the valence of any Polar extraordinary point is even. Given a triangular face $f_i$ with valence $N$, we can apply GUS on this face with vertex splitting on its Polar extraordinary point.

In order to apply GUS to $f_i$, first we need to identify its control point matrix of $\mathbf{P}$. We can index the control vertices surrounding $f_i$ as shown in Fig 3 ($f_i$ is shaded face). By Theorem 1 and (6), the $1^{st}$ layer control points in $\mathbf{P}$ is irrelevant to a deformed limit surface if we freely choose $L_1^n$ and $L_2^n$ in each GUS, then we have

$$\mathbf{P} = \begin{bmatrix} 0 & 0 & 0 & 0 \\ V & V & V & V \\ P_{31} & P_{32} & P_{33} & P_{34} \\ P_{41} & P_{42} & P_{43} & P_{44} \end{bmatrix}$$

With (5), we can derive the $5 \times 4$ GUS basis control mesh $\mathbf{P}^0$ from $\mathbf{P}$.

For each $n \geq 1$, like the situation discussed in the previous section, 2 regular sub-patches defined by a $5 \times 4$ control point matrix $\mathbf{P}^n$ will be generated by the GUS process. The last three layers $L_3^n$, $L_4^n$ and $L_5^n$ of $\mathbf{P}^n$ are obtained by performing a U-Subdivision on the first three layers of $\mathbf{P}^{n-1}$ (see Fig. 10). Hence, (6) works here as well or, equivalently,

$$\begin{bmatrix} L_3^n \\ L_4^n \\ L_5^n \end{bmatrix} = A_3 \begin{bmatrix} L_1^{n-1} \\ L_2^{n-1} \\ L_3^{n-1} \end{bmatrix} \tag{9}$$

where $A_3$ is defined in eq. (5).

The computation of $L_2^n$ involves $L_1^n$. We assume $L_1^n$ is already available to us (this is the case in the real algorithm, i.e., $L_1^n$ will be computed before the computation of $L_2^n$). $L_2^n$ is computed as follows:

$$[L_2^n] = A' \begin{bmatrix} L_1^n \\ L_1^{n-1} \\ L_2^{n-1} \\ L_3^{n-1} \end{bmatrix} \tag{10}$$

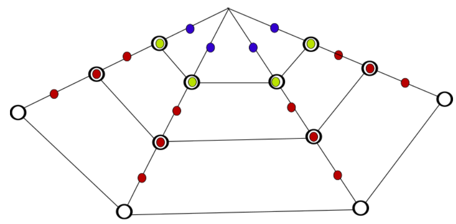

Figure 9: $\mathbf{P}^n$ (solid dots) generated after $n^{th}$ GUS, circles are the $1^{st}$ three layers of $\mathbf{P}^{n-1}$

where $A' = \begin{bmatrix} \frac{1}{4} & \frac{5}{8} & \frac{1}{8} & 0 \end{bmatrix}$. (10) is the result of a so-called *virtual U-Subdivision*. Note that, from U-Subdivision rules of (3), if we define a virtual layer of control points $L_0^{n-1}$ as follows:

$$L_0^{n-1} = 2L_1^n - L_1^{n-1}$$

and use $L_0^{n-1}$, $L_1^{n-1}$, $L_2^{n-1}$ and $L_3^{n-1}$ to form a $4 \times 4$ control mesh of a regular patch, then by performing a U-Subdivision on this $4 \times 4$ control mesh, we get a $5 \times 4$ control mesh whose first, third, fourth and fifth layers are exactly $L_1^n$, $L_3^n$, $L_4^n$ and $L_5^n$ (see Fig. 9). We call such a reverse U-Subdivision a *virtual U-Subdivision* and use the second layer of such a subdivision as the second layer of $\mathbf{P}^n$. Since $L_2^n$ corresponds to a vertex layer, we have

$$\begin{aligned} L_2^n &= \frac{1}{8}L_0^{n-1} + \frac{3}{4}L_1^{n-1} + \frac{1}{8}L_2^{n-1} \\ &= \frac{1}{4}L_1^n + \frac{5}{8}L_1^{n-1} + \frac{1}{8}L_2^{n-1} \end{aligned}$$

which is exactly (10).

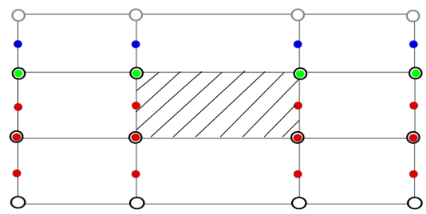

Figure 10: Virtual U-subdivision: grey circles are virtual control points, solid dots are $\mathbf{P}^n$.

**THEOREM 2:** By applying virtual U-Subdivision, limit surfaces of the two sub-patches obtained in each GUS are the same and can be considered as the limit surface of a regular patch.

*Proof* : The virtual control point layer $L_0^{n-1}$ is obtained by reversing a U-Subdivision process for edge point, such that this can be derived from PROPERTY 1.

QED

We have shown the construction of control point layers $L_2^n$, $L_3^n$, $L_4^n$ and $L_5^n$ for $\mathbf{P}^n$. We now discuss the choice of control point layer $L_1^n$.

Due to properties of GUS, the unknown control points after $n^{th}$ GUS are those in $L_1^1$, $L_1^2$, ..., and $L_1^n$. These control points determine the shape of the limit surface.

Since we expect our Polar part at V is at least $C^1$ (tangent plane continuous) with common data point $d_V$ at (0,v) and common unit normal $n_V$ at $d_V$, we have the following proposition for $G^2$ continuous at V,

**PROPOSITION 1**: For any $f_i$ and $f_{i+\frac{N}{2}}$ on the opposite side of Polar extraordinary point V, if each control point in $L_1^n$ of $f_i$ and its corresponding control point in $L_1^n$ of $f_{i+\frac{N}{2}}$ are on a $C^2$ curve across $d_V$ and share the same unit normal $n_V$, then if basis control mesh $\mathbf{P}^0$ does not appear in derivatives of any Polar parametric subdivision surface patch at $d_V$ up to the $2^{nd}$ order, then it is $G^2$ at Polar extraordinary point V.

**PROOF**: The proof is trivial. If basis control mesh $\mathbf{P}^0$ does not appear in derivatives of any Polar parametric subdivision surface patch at $d_V$ up to the $2^{nd}$ order, it means that control points of $\mathbf{P}^0$ do not appear in derivative polynomials at $n^{th}$ GUS limit surface up to the $2^{nd}$ order, when $n \to \infty$. By construction of GUS, then in the derivative polynomials only control points of $L_1^n$ matters. Due to the symmetry of control points and all corresponding control points in $L_1^n$ of $f_i$ and $f_{i+\frac{N}{2}}$ form a $C^2$ curve across $d_V$ and share same unit normal $n_V$, an arbitrary control point in $\mathbf{P}^n$ of $f_i$ must be on a $C^2$ curve across $d_V$ with its corresponding control point in $\mathbf{P}^n$ of $f_{i+\frac{N}{2}}$ (a linear combination of a set of $C^2$ curves across $d_v$ and share the same unit normal $n_V$ must be a $C^2$ curve across $d_V$ and have the unit normal $n_V$ ). Since a data point at (u,0) of $f_i$ at the $n^{th}$ GUS is generated by affine combination of its control points in $\mathbf{P}^n$, with the symmetric arrangement of $f_i$ and $f_{i+\frac{N}{2}}$, we can show that the arbitrary corresponding data points at the limit surface of $n^{th}$ GUS of $f_i$ and $f_{i+\frac{N}{2}}$ are on a $C^2$ curve across $d_V$ and have the same unit normal $n_V$. QED

From Proposition 1, we expect for an arbitrary Polar patch $f_k$, each control point in $L_1^n$ shall be on a $C^2$ curve with its opposite control point in $f_{k+\frac{N}{2}}$, this $C^2$ curve shall be across $d_V$ and have a unit normal $n_V$ at $d_V$.

From this expectation, before picking the unknown values $L_1^1$, $L_1^2$,...,$L_1^n$ of the GUS's, we have to first determine the values of $d_V$ and $n_V$. If we reorganize the control points surrounding V as $\{V, E_1, E_2, ..., E_N\}$, where $E_1, ...E_N$ are edge points connected to the extraordinary point V in a counterclockwise order, and define the triangular face $f_k$ by $\{V, E_k, E_{k\%N+1}\}$, $k \in [1, N]$, we can pick the values of these terms as follows:

$$d_V = \frac{2}{3}V + \frac{1}{3N}\sum_{k=1}^{N} E_k$$
$$n_V = Norm(\sum_{k=1}^{N} n_{f_k}) \qquad (11)$$

where Norm(x) is a function which returns unit normal of a normal x. $n_{f_k}$ is the face normal of $f_k$, can be obtained from $n_{f_k} = (E_k - V) \times (E_{k\%N+1} - V)$.

We notice that CCS regular patch (Fig 5 left) is $C^2$ continuous at V, so new $E_1$ and $E_3$ at $n^{th}$ CCS must be on a $C^2$ curve that across the limit point $d_V$ of $V$ and lies on the tangent plane of CCS limit surface at $d_V$. This inspires us to come up with the concept of *dominative control meshes*. A *dominative control mesh* $C_m$ of size 9 is defined as

$$C_m = [V_m, E_{m,1}, \ \dots, E_{m,4}, F_{m,1}, \ \dots, F_{m,4}]^T,$$

which is exactly the control point mesh of a regular bicubic patch without $[I_1, I_2, I_3, I_4, I_5, I_6, I_7]^T$.

By applying midpoint knot insertion to $C_m$, we get

$$C_m^{(n)} = A_9 C_m^{(n-1)} = ... = (A_9)^n C_m, n \geq 1 \qquad (12)$$

where $A_9$ is the midpoint insertion coefficient matrix, its values can be derived from eq. (1). $C_m^{(n)}$ is the control point mesh after $n^{th}$ midpoint knot insertion on $C_m$, and can be expressed as

$$C_m^{(n)} = [V_m^{(n)}, E_{m,1}^{(n)}, \ \dots, E_{m,4}^{(n)}, F_{m,1}^{(n)}, \ \dots, F_{m,4}^{(n)}]^T$$

The reason $I_i (i = 1, ..., 7)$ are ignored is: as shown in (1), the new vertex point, edge points and face points obtained from the midpoint knot insertion are independent of these inner ring control vertices. Since we plan to map recursively generated edge points of dominative control meshes into unknown values of $L_1^n$ in GUS's, it will not be necessary to include these vertices into the control mesh.

There are totally N faces surrounding V, so we need N dominative control meshes to map these values, see Fig. 11 for the mapping from the dominative control meshes to the control points of the $n^{th}$ GUS on face $f_k$. The mapping is defined as follows:

$$L_1^n[1] = E_{k-1,1}^{(n+1)}; \qquad L_1^n[2] = E_{k,1}^{(n+1)};$$
$$L_1^n[3] = E_{k+1,1}^{(n+1)}; \qquad L_1^n[4] = E_{k+2,1}^{(n+1)} \qquad (13)$$

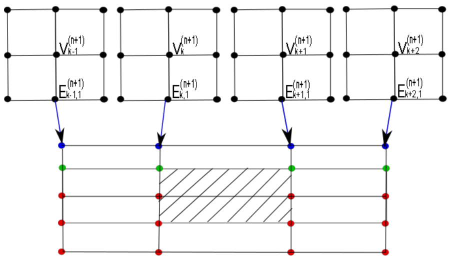

Figure 11: Mapping the recursively generated control points in dominative control meshes to $L_1^n$ of $n^{th}$ GUS on $k^{th}$ face $f_k$.

Due to the ring structure of control points in GUS, for the $n^{th}$ GUS, the last three points in $L_1^n$ of $f_{k-1}$ are exactly the first three points in $L_1^n$ of $f_k$. Hence, for each $f_k$, we only need to consider the mapping from $E_{k,1}^{(n+1)}$ to $L_1^n[2]$ and, yet, we get all the control points for each $L_1^n$ once this mapping is considered for all $k$.

To get the values of $L_1^n[2]$ $(n \geq 1)$ for $f_k$, we initialize the dominative control mesh $C_k$ as follows:

$$
\begin{aligned}
E_{k,1} &= E_k; & E_{k,3} &= E_{k+\frac{N}{2}};\\
F_{k,1} &= E_{k+1}; & F_{k,2} &= E_{k+\frac{N}{2}-1};\\
F_{k,3} &= E_{k+\frac{N}{2}+1}; & F_{k,4} &= E_{k-1};
\end{aligned}
$$

As mentioned before, we treat a triangular face as a special case of a quad face by vertex splitting. Let $E_{k,2}$=$E_{k,4}$=$V_k$. Then we have:

$$V_k = E_{k,2} = E_{k,4} = \frac{3}{2}(d_V - \frac{1}{9}(E_{k,1} + E_{k,3}) - \frac{1}{36}\sum_{i=1}^{4} F_{k,i})$$

This initialization guarantees that the limit point of the dominative control mesh equals $d_V$ . In order to make the GUS surface is tangent plane continuous at the extraordinary point, we will further process the dominative control meshes such that they have the same unit normal $n_V$ at the limit data point. The algorithm is as follows:

**(1)** get the first order derivatives $D_u$, $D_v$ at $d_{V_k}$. Since $C_k$ is a part of a regular patch, it can be easily calculated.

**(2)** get $t = D_u \cdot n_V$, the projection of $D_u$ on $n_V$

**(3)** let $F_{k,1}- = 3t$, $F_{k,4}- = 3t$, $F_{k,2}+ = 3t$, $F_{k,3}+ = 3t$, which ensure $D_u \cdot n_V = 0$

**(4)** get $t = D_v \cdot n_V$, the projection of $D_v$ on $n_V$

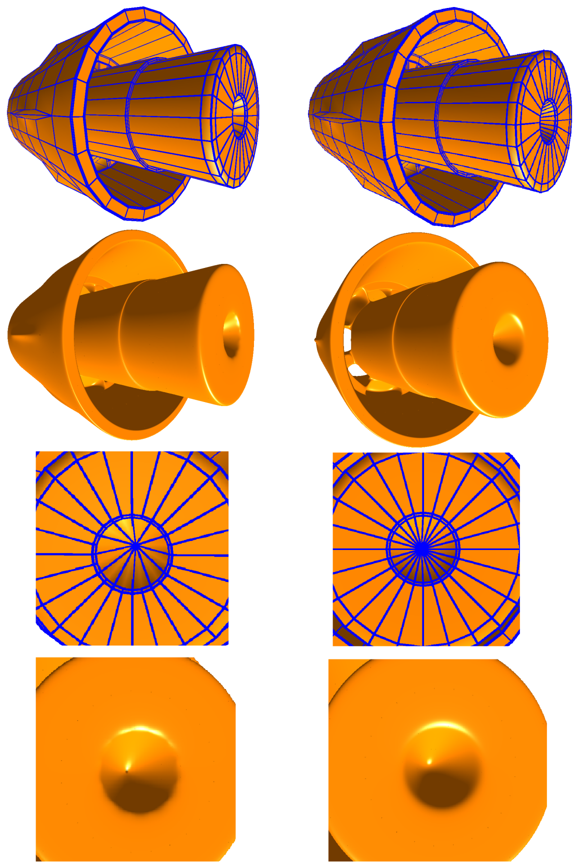

Figure 12: left: original CCS mesh and its limit surface, right: revised PCC mesh and its limit surface. The bottom left photo shows irregularity at boundaries of high-valence CCS extraordinary faces, and the bottom right is smooth.

**(5)** let $F_{k,1}- = 3t$, $F_{k,2}- = 3t$, $F_{k,3}+ = 3t$, $F_{k,4}+ = 3t$, which ensure $D_v \cdot n_V = 0$

From above algorithm and initialization, since $N$ is even, the opposite dominative control meshes $C_k$ and $C_{k+\frac{N}{2}}$ will share the same set of control points, differing only in the ordering.

With all control points in $L_1^n$ defined in (13), we are now complete with the selection process for control points in $\mathbf{P}^n$. Let us reinstate (8) of parameterization surface at $f_k$ as follows:

$$S(k, u, v) = W^T(u)K^n D_b M S_b \mathbf{P}^n M^T W(v) \qquad (14)$$

$$\mathbf{P}^n = A_5\mathbf{P}^{n-1} + S_5 A_9^{n+1} T_k, \quad n \geq 1 \tag{15}$$

$$with\ A_5 = \begin{bmatrix} 0 & 0 & 0 & 0 & 0 \\ \frac{5}{8} & \frac{1}{8} & 0 & 0 & 0 \\ \frac{1}{2} & \frac{1}{2} & 0 & 0 & 0 \\ \frac{1}{8} & \frac{3}{4} & \frac{1}{8} & 0 & 0 \\ 0 & \frac{1}{2} & \frac{1}{2} & 0 & 0 \end{bmatrix}, S_5 = \begin{bmatrix} 0&1&0&0&0&0&0&0&0 \\ 0&\frac{1}{4}&0&0&0&0&0&0&0 \\ 0&0&0&0&0&0&0&0&0 \\ 0&0&0&0&0&0&0&0&0 \\ 0&0&0&0&0&0&0&0&0 \end{bmatrix},$$

$$\mathbf{P}^0 = \begin{bmatrix} A_3 P'_{3,4}\mathbf{P} \\ 0 \end{bmatrix},$$

$T_k = [C_{k-1}\ C_k\ C_{k+1}\ C_{k+2}]$, is a matrix of size $9 \times 4$, with each column representing one of the four dominative control meshes related to $f_k$. $A_9$ is defined in eq. (12).

In this section, we have shown how to construct a GUS surface on Polar triangular faces in a PCC mesh. In next section, we will show the behavior of the PCC surfaces.

## 6. Evaluating the PCC surface

A PCC surface composes of two parts, CCS part and Polar part. For the CCS part, the behavior of the limit surface was already covered in [2]. In this section, we focus on the behavior of the limit surface on Polar part.

As shown in the previous sections, a GUS surface of a triangular face is $C^2$ on the limit surface and also $C^2$ continuous with its adjacent quad faces. We will now evaluate the surface at Polar extraordinary points.

(15) is a recursive formula , the evaluation of the GUS surface at Polar extraordinary point needs an explicit expression for $\mathbf{P}^n$. We can expand (15) as follows:

$$\begin{aligned} \mathbf{P}^n \quad &= A_5^n \mathbf{P}^0 + A_5^{n-1} S_5 A_9^2 T_k + A_5^{n-2} S_5 A_9^3 T_k + ... \\ &\quad + A_5 S_5 A_9^n T_k + S_5 A_9^{n+1} T_k \\ &= A_5^n \mathbf{P}^0 + \sum_{i=1}^{n} A_5^{n-i} S_5 A_9^{i+1} T_k \quad n \geq 1 \end{aligned} \tag{16}$$

$A_5$ has a single eigenvalue of $\frac{1}{8}$, and has the following properties:

$$A_5 \quad = \frac{1}{8} \begin{bmatrix} 0&0&0&0&0 \\ 5&1&0&0&0 \\ 4&4&0&0&0 \\ 1&6&1&0&0 \\ 0&4&4&0&0 \end{bmatrix}, \quad A_5^2 = \frac{1}{8}^2 \begin{bmatrix} 0&0&0&0&0 \\ 5&1&0&0&0 \\ 20&4&0&0&0 \\ 34&10&0&0&0 \\ 36&20&0&0&0 \end{bmatrix},$$

$$A_5^n \quad = \frac{1}{8}^n \begin{bmatrix} 0&0&0&0&0 \\ 5&1&0&0&0 \\ 20&4&0&0&0 \\ 50&10&0&0&0 \\ 100&20&0&0&0 \end{bmatrix} = \frac{1}{8}^n \Theta, \quad n \geq 3$$

$A_9$ is a $9 \times 9$ regular midpoint insertion coefficient matrix, its eigenstructure is studied in an earlier work on CCS surfaces [3] [18]. The eigenvalues of $A_9$ are 1, $\frac{1}{2}$, $\frac{1}{4}$, $\frac{1}{8}$ and $\frac{1}{16}$, and we define their corresponding eigenbases as $\Theta_1$, $\Theta_2$, $\Theta_3$, $\Theta_4$ and $\Theta_5$, with

$$A_9^n = \Theta_1 + \frac{1}{2}^n \Theta_2 + \frac{1}{4}^n \Theta_3 + \frac{1}{8}^n \Theta_4 + \frac{1}{16}^n \Theta_5$$

Thus, when $n \geq 3$, (16) can be rewritten as:

$$\begin{aligned} \mathbf{P}^n \quad &= \frac{1}{8}^n \Theta \mathbf{P}^0 + S_5 A_9^{n+1} T_k + A_5 S_5 A_9^n T_k + A_5^2 S_5 A_9^{n-1} T_k \\ &\quad + \sum_{i=1}^{n-3} \frac{1}{8}^{n-i} \Theta S_5 (\Theta_1 + \frac{1}{2}^{i+1} \Theta_2 + \frac{1}{4}^{i+1} \Theta_3 \\ &\quad + \frac{1}{8}^{i+1} \Theta_4 + \frac{1}{16}^{i+1} \Theta_5) T_k, \end{aligned} \tag{17}$$

Take (17) into Polar parametric surface of (14), because its coefficient is $\frac{1}{8}^n$, such that it will be zero in derivatives up to the $2^{nd}$ order when $n \to \infty$.

From Proposition 1, we now can conclude that the limit surface generated by our new scheme on Polar part will be curvature continuous at the Polar extraordinary points.

## 7. Discussion and Conclusion

In this paper, a new subdivision scheme with Polar embedded Catmull-Clark mesh structure is introduced. By introducing Polar configuration on high valence vertex, the ripple problem inherent in a CCS surface is solved.

The subdivision scheme developed has the properties that the limit surface on the CCS part is exactly the same as a CCS limit surface and the limit surface on the Polar part is $G^2$ continuous everywhere.

Since it is inevitable to have high valence extraordinary points in some cases, e.g. airplanes, rockets and engineering parts, the currently available CCS meshes can be easily converted to PCC meshes, such that one can avoid redesigning the complete mesh.

In contrast to commonly used Polar subdivision rules, the subdivision masks of proposed GUS subdivision scheme on Polar part is equivalent to those of CCS. The properties of GUS surfaces are studied and proven. The GUS scheme is a stationary scheme.

The curvature at a Polar extraordinary point is independent of nearby control points, but relies on some selected dominative control meshes. Implementation results (Fig 12) show that very high quality, curvature continuous subdivision surfaces can be generated with this

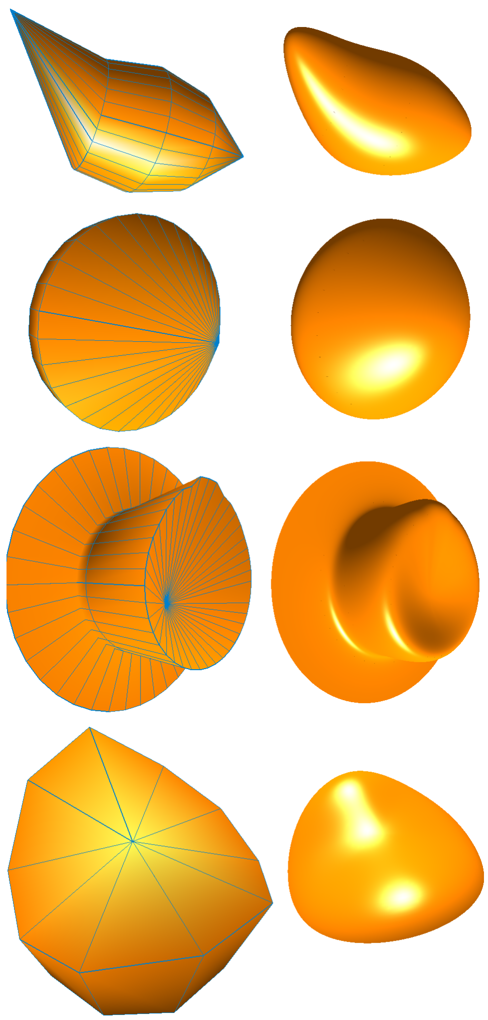

Figure 13: Various primitives of GUS surfaces on Polar parts

new scheme on the Polar part. Furthermore, the scheme is WYSIWYG (what you see is what you get): as far as the ring of control points connected around the Polar extraordinary point is smooth, there will be no ripples.

Our next step is to develop a general geometric framework to incorporate some $G^2$ schemes for CCS meshes into the PCC subdivision scheme, so that a $G^2$ everywhere PCC surface can be generated.

## References


[1] E. Catmull, J. Clark, Recursively generated B-spline surfaces on arbitrary topological meshes, Computer-Aided Design 10 (6) (1978) 350–355.

[2] D. Doo, M. Sabin, Behaviour of recursive division surfaces near extraordinary points, Computer-Aided Design 10 (6) (1978) 356–360.

[3] J. Stam, Exact evaluation of Catmull-Clark subdivision surfaces at arbitrary parameter values, in: Proceedings of the 25th annual conference on Computer graphics and interactive techniques, ACM, 1998, p. 404.

[4] H. Prautzsch, Smoothness of subdivision surfaces at extraordinary points, Advances in Computational Mathematics 9 (3) (1998) 377–389.

[5] A. Levin, Modified subdivision surfaces with continuous curvature, ACM Transactions on Graphics (TOG) 25 (3) (2006) 1040.

[6] K. Karciauskas, J. Peters, Concentric tessellation maps and curvature continuous guided surfaces, Computer Aided Geometric Design 24 (2) (2007) 99–111.

[7] C. Loop, S. Schaefer, G2 tensor product splines over extraordinary vertices, in: Computer Graphics Forum, Vol. 27, John Wiley & Sons, 2008, pp. 1373–1382.

[8] M. Halstead, M. Kass, T. DeRose, Efficient, fair interpolation using catmull-clark surfaces, in: Proceedings of the 20th annual conference on Computer graphics and interactive techniques, ACM, 1993, pp. 35–44.

[9] J. Peters, K. Karčiauskas, An introduction to guided and polar surfacing, Mathematical Methods for Curves and Surfaces (2010) 299–315.

[10] K. Karčiauskas, J. Peters, Bicubic polar subdivision, ACM Transactions on Graphics (TOG) 26 (4) (2007) 14.

[11] P. J. Myles A., Bi-3 c2 polar subdivision, ACM Trans. Graph 28 (3) (2009) 1–12.

[12] A. Myles, K. Karčiauskas, J. Peters, Pairs of bi-cubic surface constructions supporting polar connectivity, Computer Aided Geometric Design 25 (8) (2008) 621–630.

[13] J. Peters, L. Shiue, Combining 4-and 3-direction subdivision, ACM Transactions on Graphics (TOG) 23 (4) (2004) 980–1003.

[14] J. Stam, C. Loop, Quad/triangle subdivision, in: Computer Graphics Forum, Vol. 22, Wiley Online Library, 2003, pp. 79–85.

[15] S. Schaefer, J. Warren, On c 2 triangle/quad subdivision, ACM Transactions on Graphics (TOG) 24 (1) (2005) 28–36.

[16] A. Myles, curvature-continuous bicubic subdivision surfaces for polar configurations (2008).

[17] A. Ball, D. Storry, Conditions for tangent plane continuity over recursively generated B-spline surfaces, ACM Transactions on Graphics (TOG) 7 (2) (1988) 102.

[18] S. Lai, F. Cheng, Similarity based interpolation using Catmull–Clark subdivision surfaces, The Visual Computer 22 (9) (2006) 865–873.